PAPER • OPEN ACCESS

Multi-wavelength 128 Gbit s^{-1} λ^{-1} PAM4 optical transmission enabled by a 100 GHz quantum dot mode-locked optical frequency comb

Multi-wavelength 128 Gbit s^{-1} λ^{-1} PAM4 optical transmission enabled by a 100 GHz quantum dot mode-locked optical frequency comb

Shujie Pan[1,*], **Hongguang Zhang**[2], **Zizhuo Liu**[1], **Mengya Liao**[1], **Mingchu Tang**[1], **Dingyi Wu**[2], **Xiao Hu**[2], **Jie Yan**[2], **Lei Wang**[2], **Mingchen Guo**[3], **Zihao Wang**[3], **Ting Wang**[3], **Peter M Smowton**[4], **Alwyn Seeds**[1], **Huiyun Liu**[1], **Xi Xiao**[2] and **Siming Chen**[1,*]

[1] Department of Electronic and Electrical Engineering, University College London, Torrington Place, London WC1E 7JE, United Kingdom
[2] National Information Optoelectronics Innovation Center, China Information and Communication Technologies Group Corporation (CICT), Wuhan 430074, People's Republic of China
[3] Beijing National Laboratory for Condensed Matter Physics, Institute of Physics, Chinese Academy of Sciences, Beijing 100190, People's Republic of China
[4] Department of Physics and Astronomy, Cardiff University, Queens Building, The Parade, Cardiff CF24 3AA, United Kingdom

E-mail: shujie.pan.14@ucl.ac.uk and siming.chen@ucl.ac.uk

CrossMark

Abstract
Semiconductor mode-locked lasers (MLLs) with extremely high repetition rates are promising optical frequency comb (OFC) sources for their usage as compact, high-efficiency, and low-cost light sources in high-speed dense wavelength-division multiplexing transmissions. The fully exploited conventional C- and L- bands require the research on O-band to fulfil the transmission capacity of the current photonic networks. In this work, we present a passive two-section InAs/InGaAs quantum-dot (QD) MLL-based OFC with a fundamental repetition rate of ∼100 GHz operating at O-band wavelength range. The specially designed device favours the generation of nearly Fourier-transform-limited pulses in the entire test range by only pumping the gain section while with the absorber unbiased. The typical integrated relative intensity noise of the whole spectrum and a single tone are −152 and −137 dB Hz^{-1} in the range of 100 MHz–10 GHz, respectively. Back-to-back data transmissions for seven selected tones have been realised by employing a 64 Gbaud four-level pulse amplitude modulation format. The demonstrated performance shows the feasibility of the InAs QD MLLs as a simple structure, easy operation, and low power consumption OFC sources for high-speed fibre-optic communications.

Keywords: quantum-dot, mode-locked laser, optical frequency combs

(Some figures may appear in colour only in the online journal)

---

1. Introduction

The optical frequency combs (OFCs) with a straightforward connection between optical and microwave domains are used in numerous fields, such as medical diagnostics [1], atomic clock distribution/recovery [2], precision measurements [3–5], gas spectroscopy [6, 7], and optical communications [8–12]. To support such a broad application divergence, the last two decades have witnessed an expansion of the laser-based comb technology [13, 14]. There are various OFC generation mechanisms, including gain switched comb, nonlinear fibres, microresonator systems, electro-optic comb generators, and mode-locked lasers (MLLs). Among all technologies, the MLLs, particularly the semiconductor MLLs, are considered the most promising light sources in future photonic integrated circuits (PICs) owing to their simplification, compactness, easy-operation, low power consumption, and high wall-plug efficiency [9, 15].

Although, quantum-well materials have been intensively investigated over the last two decades. The quantum-dot (QD) material, benefits from a broader inhomogeneous gain spectrum, an ultrafast carrier dynamic [16], together with other inherent features like low threshold current [17], temperature resilience [18, 19], high tolerance to defects and optical feedback [28, 29] have attracted increasing attentions and offered opportunities for future complementary metal-oxide-semiconductor (CMOS)-compatible PIC technology [30–34].

During the past decade, the ever-growing demand for data transmission capacities have inspired the research in dense wavelength-division multiplexing (DWDM) technology. The ITU-T G.694.1 recommendation has proposed a variety of fixed channel spacings ranging from 12.5 to 100 GHz in DWDM applications. While the MLLs-based OFC sources with a larger mode-spacing ($\geqslant$100 GHz) are more desirable in the DWDM transmission systems for the potentially reduced number of light sources required, it is challenging to obtain the needed high gain in an ultimate short cavity, especially for QD materials devices. Given that, most previous QD-based mode-locked OFC studies (as summarised in table 1) have either involved complex high order harmonics [21, 27], or employed complicated system-level setups [25] for large mode-spacing OFC generations. It is notable that most high-performance devices operate at the telecom C-band, while the devices working at telecom O-band are still relatively immature, suffering from a lower modal gain and a broader pulse duration. Furthermore, the conventional C-band has been extensively exploited, the current state-of-the-art high-speed transmission system requires the use of telecom O-band to boost the transmission capacity of existing photonic networks [35].

Considering all points listed above, in this work, we report a passively QD MLL-based O-band transform-limited OFC source generated at ∼100 GHz fundamental repetition rate with sub-picosecond pulse durations. By optimising the growth conditions, a QD active region with high dot density (5.9 × 10¹⁰ cm⁻²) and good uniformity is accomplished, providing a room-temperature PL full width at half-maximum (FWHM) as low as 28 meV. During the

whole test range, nearly Fourier-transform-limited Gaussian-pulses with ∼100 GHz mode-spacing are realised throughout. The typical integrated average relative intensity noise (RIN) values of the whole spectrum and a single tone, average between 100 MHz and 10 GHz, are −152 and −137 dB Hz⁻¹, respectively. Moreover, the transmission ability of this laser is evaluated by carrying out a 64 Gbaud four-level pulse amplitude modulation (PAM-4) back-to-back (B2B) transmission for seven independent channels. The corresponding measured bit error ratios (BERs) confirm the possibilities for such OFC source usage in high-speed data centre applications. Our results suggest the proposed two-section QD MLL is a powerful candidate for simple structure, low-cost, high efficiency and integrable DWDM light sources.

2. Material and device design

The devices presented in this paper were prepared by solid-state molecular beam epitaxy, with emission wavelength in the 1.3 μm range. A self-assembled InAs QD structure was grown on a Si-doped GaAs (001) surface together with AlGaAs cladding layers. Here, a high-quality 300 nm Si-doped GaAs contact layer was first developed, followed by the lower cladding layer that consists of n-type $Al_{0.2}Ga_{0.8}As/Al_{0.4}Ga_{0.6}As/Al_{0.2}Ga_{0.8}As$ in a thickness of 20 nm/1400 nm/20 nm, respectively. Then, the active region containing an eightfold layer stack of InAs QDs was situated in the centre of the lower and upper cladding layers. The upper cladding layer was comprised of p-type $Al_{0.2}Ga_{0.8}As/Al_{0.4}Ga_{0.6}As/Al_{0.2}Ga_{0.8}As$ in a thickness of 20 nm/1400 nm/20 nm. After depositing a heavily p+-doped 300 nm thick GaAs contact layer above the upper cladding layer, the entire growth procedure was completed. As known, a high optical gain is a prerequisite for ultra-high repetition rate pulse generation in a two-section passively MLL. To this end, an extraordinary design is utilised in the active region to improve the material's performance. The inset of figure 1(a) shows the cross-sectional TEM image of the active region. A larger than a usual number of QD layers (eight layers in total) was employed to obtain the desired high optical gain. Instead of using the conventional dot-in-a-well structure, here, the QDs were self-assembly formed by depositing three monolayers of InAs directly on the GaAs surface. Then, the initial QDs were covered by a 3.7 nm strain-reducing layer made of InGaAs. Such strain-reduced QDs could promise the light emission at the range of 1.3 μm, maintain the high QD density while preserving the QDs uniformity [36, 37]. The profile of a single dot can be extracted from the zoom-in window, where a high-resolution TEM image showing a truncated pyramidal shaped QD with a base length of 20–25 nm and a height of 6–8 nm. As a result, an ultrahigh dot density of 5.9 × 10¹⁰ cm⁻² (nearly double the previous result of 3 × 10¹⁰ cm⁻² [38]) is finally accomplished in this multi-layer structure with no degradation in QD uniformity. The room-temperature PL emission spectrum with a narrow linewidth of 28 meV is displayed in figure 1(a), indicating a minor variation in size and shape of inhomogeneous QDs in this work.

Table 1. Summary of QD-based mode-locked OFC source with an ultrahigh repetition rate.

Telecom band	Repetition rate (GHz)	Material	Methods	Pulse duration (ps)	−3 dB bandwidth (nm)	TBP Gaussian	Sech^2	Year/ references
C-band	134	InGaAsP/InAs QDash	Single section	0.8	4.3	0.46	—	2006/[20]
O-band	117	InGaAs QD	CPM-3rd harmonic	2.14	—	—	0.39	2006/[21]
	238		CPM-6th harmonic	1.3	—	—	0.33	
C-band	92	InAs/InP QD	Single section	0.312	11.62	0.457	—	2008/[22]
C-band	10–100	InAs/InP QD	Single section	0.295	17.9	0.66	—	2010/[23]
	437		FBGs	0.810	—	—	—	
O-band	100	InGaAs/GaAs QD	Mode-selections	—	—	—	—	2010/[24]
O-band	100	InGaAs/GaAs QD	Fabry–Perot Etalon	—	—	—	—	2011/[25]
O-band	102	QD	CPM-6th harmonic	—	—	—	—	2018/[26]
O-band	100	Chirped QD	CPML-5th harmonic	2.3	—	—	—	2019/[27]
O-band	94	InGaAs/GaAs QD	Two-section	0.69	3.18	0.45	—	This work
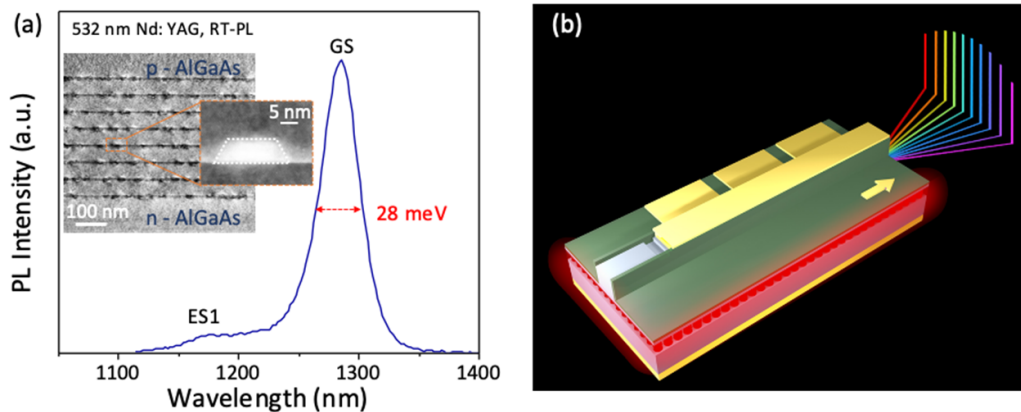
Figure 1. (a) The room-temperature photoluminescence (PL) emission spectrum of the sample. (Inset: the cross-sectional transmission electron microscopy (TEM) image of the active region and a single dot (zoom-in)). (b) Schematic of the unbiased passively two-section MLL.

The schematic diagram of the device under investigation is presented in figure 1(b). The 5 μm wide two-section MLLs were processed from the wafer described above with standard fabrication methods, including semiconductor dry etching and metal/dielectric deposition techniques. Based on the previous study with a similar structure in [19], a group effective index of 3.7 can be found. To realise ∼100 GHz mode-spacing, the total cavity length of the lasers was set to be 405 μm, 14% (56.7 μm) of which formed the saturable absorber (SA) section. Such design could provide us with a comparable high differential loss in the SA section and a relatively small differential gain in the gain section, resulting a high gain-to-SA saturation energy ration in this extremely short cavity device. A citric-acid solution was used to selectively remove a width

of 10 μm of the heavily doped p-type contact GaAs layer between the gain and SA sections, achieving an electrical isolation resistance of around 2.5 kΩ. After thinning the backside to 120 μm, a high-reflective coating of 95% was applied on the facet close to the SA section while the facet near the gain section was left to as-cleaved. Then, the lasers were mounted p-side up on an indium-plated copper heat sink and gold-wire-bonded to enable electrical contacts. Finally, the devices were packaged with a thermoelectric temperature controller (TEC) controller to fix the heat sink temperature at 20 °C. It is worth mentioning that, mode-locking (ML) phenomenon was obtained without reversed bias applied to the SA section, therefore, those unbiased two-section devices were packaged similarly to a single-section self-mode-locked (SML) laser
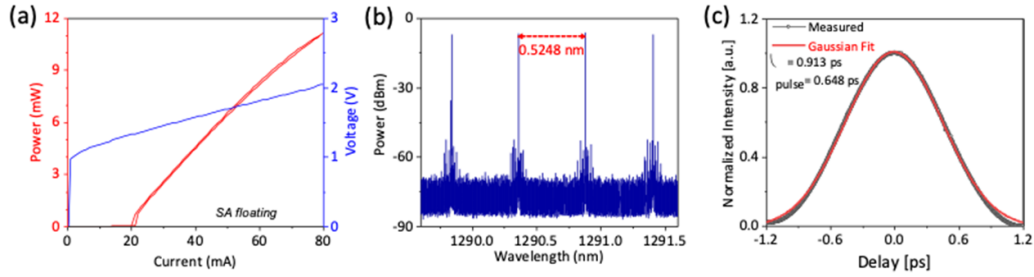
Figure 2. Two-section unbiased QD MLL basic characterisation at room temperature: (a) continuous wave L–I–V curve with SA floating. (b) High-resolution optical spectrum for adjacent channels (resolution: 0.04 pm). (c) Autocorrelation trace with Gaussian pulse fitting.

since the minimal absorption will not affect the self-ML mechanism [39, 40].

3. Characterisation and discussion

3.1. Mode-locking (ML) performance

The MLLs used in this experiment operating as SML lasers since their SA sections were left floating [41]. To study their behaviours, the output spectrum was measured using an optical spectrum analyser (OSA) (Yokogawa AQ6370D or APEX AP2087A), and the pulse width was recorded with APE pulseCheck autocorrelator. Figure 2 summarises the representative continuous-wave characteristics of fabricated devices at room temperature. The measured light–current–voltage (*L–I–V*) curve is displayed in figure 2(a). The *L–I* curve presents the dependence of the average power received by a broad area detector on the bias current for gain sections, where 20 mA threshold current (I_{th}) and 17.7% slope efficiency is exhibited. The test is stopped at 80 mA, taking into account the strong possibility of a damaged ultra-short cavity laser under a high-power density condition. As noticed, when injected current (I_{gain}) increases from the I_{th}, output power increases; when I_{gain} decreases after reaching the maximum value, the laser power decreases, but it persists even if $I_{gain} < I_{th}$. This results in a hysteresis loop near the I_{th}, indicating the bistability of these devices [32]. As for the *I–V* curve, it exhibits a typical behaviour of a semiconductor laser where the voltage increases gradually with increased I_{gain}.

The mode-spacing of adjacent tones, i.e. the repetition rate of the device, is evaluated through *apex* OSA with a 0.04 pm resolution. In figure 2(b), the optical spectrum of four tones located near the central wavelength of 1291 nm at 66 mA is shown. A mode-spacing of 0.5248 nm is obtained, corresponding to a fundamental repetition rate of 94.6 GHz. To the best of our knowledge, this is the highest fundamental mode-spacing ever-achieved by a single QD-MLL in telecom O-band. Figure 2(c) shows the autocorrelation signal of an isolated pulse under the same bias condition to confirm the ML regime. The measured pedestal-free pulse profile is in good agreement with the fitted Gaussian pulse shape and gives a 648 fs deconvolved pulse duration without any external pulse compression scheme.

Figure 3(a) highlights the trends observed in the OSA spectrum evolution for I_{gain} increment. The observations are refined and presented more visually in figure 3(b). By increasing the I_{gain} from 20 to 80 mA, a continuously red-shift of centre wavelength (from 1288 to 1293 nm) can be seen, confirming sustained ground state lasing. Meanwhile, the OSA spectrum tends to become a multipeak structure with an additional peak occurs in the high-frequency side due to an increased degree of self-phase modulation with increasing carrier density [42]. Hence, resulting in a steady expansion of OSA 3 dB bandwidth (from 1.6 to 4.3 nm).

This phenomenon has also been reported by other research groups [32, 43]. And we believe such a current-induced red-shift tendency could be minimised by carefully tailoring the structure of QDs [44, 45]. The corresponding pulse-duration obtained at each current level together with the calculated TBP values are given in figure 3(c). Considering the average output power at a low driving current is not directly measurable from the autocorrelator (AC). We, therefore, employed a praseodymium-doped fiber amplifier (PDFA) to maintain the laser average power at the ∼6 dBm level. Normally, the ML pulse duration is relatively sensitive to both driving current and reverse-bias voltages. The shortest pulse durations are commonly observed at high reverse-bias voltages and low driving currents (∼I_{th}), while any deviations away from these optimum driving conditions will deteriorate pulse width [32, 46–49]. Albeit unusual, some research groups have reported the shortest pulse generation under the condition of high reverse-bias voltages and I_{gain} far beyond the I_{th} [50, 51]. Despite that, neither trend holds in our case, where a continuous pulse shortening mechanism relies solely on I_{gain} increment, without the need for a voltage source. Consequently, the shortest pulse (∼466 fs) is obtained at the upper-limit of our test range. The possible reason could be the change of the short-pulses generation mechanism within the two-section lasers [52, 53]. Also evident from figure 3(c), the small fluctuations of calculated TBP with an average value of 0.472 indicating the nearly transform-limited nature of the pulses during the whole ML regime.

3.2. Data transmission experiment and results

To verify our QD MLLs are feasible for high-speed communications, a system-level WDM experiment using PAM-4
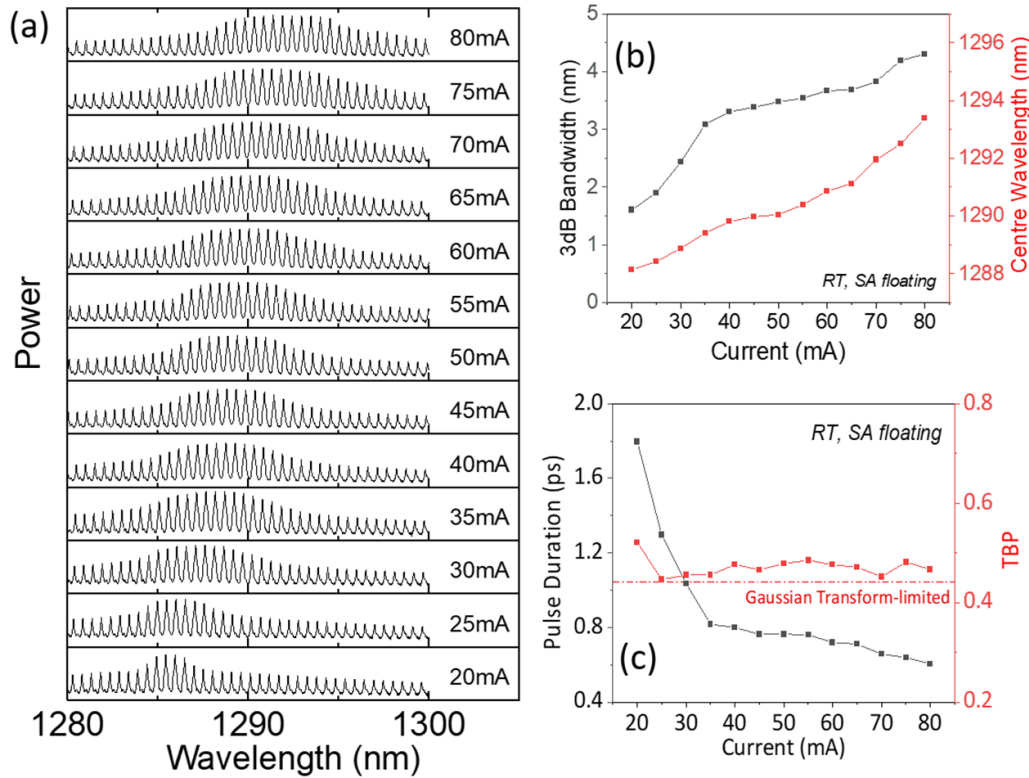
Figure 3. Room-temperature characteristics of two-section unbiased passively QD MLL with SA floating and I_{gain} from 20 to 80 mA. (a) Optical spectra (resolution: 0.02 nm). (b) Spectral width and centre wavelength in (a). (c) Pulse duration and corresponding calculated TBP value.

modulation format is performed. The experimental setup is depicted in figure 4(a). Each wavelength channel generated by QD MLLs can be considered as an optical carrier. And the channel we interest in will be selected by a tunable band pass filter (OBPF) (EXFO XTM-50). After selection, the carrier power is boosted from approximately −7 dBm to around +14 dBm by an O-band optical amplifier (FiberLabs Inc. AMP-FL8611-OB-16). Then, the amplified optical carrier signal is launched into a 40 GHz lithium niobate MZM (iXblue MX1300-LN-40) for data modulation. Notably, in our case, no extra OBPF is employed to suppress out-of-band amplified spontaneous emission (ASE) after the PDFA due to the great insertion loss at a low FWHM level (∼10 dB). The modulator is driven by an AWG (Keysight M8194A, with 50 GHz bandwidth and 120 GSa s^{-1}), where a 64 Gbaud pseudo-random binary sequence 2^{15}–1 pattern with a length of 32 767 bits is generated in PAM-4 format. And the AWG-generated electrical PAM-4 signals are amplified to approximately 3 V peak-to-peak by a 55 GHz broadband radio-frequency (RF) amplifier (SHF S807C). Following the modulator, a VOA is added before the 50 GHz PD (Finisar XPDV2320R) to control the received optical power. Another RF amplifier is utilised to enhance the amplitude of the electrical signal. The received signal is digitally captured by a 70 GHz real-time oscilloscope (Keysight UXR0704A) with a sampling rate of 256 GS s^{-1}. Finally, an offline DSP similar to that described in [54] is carried out for signal demodulation and BER evaluation.

Figure 4(b) shows the optical spectrum under the bias condition of $I_{gain} = 66$ mA, which exhibits a centre wavelength of 1290.755 nm and a 3 dB comb bandwidth of 3.46 nm. A total number of 7 carriers lie within the 3 dB bandwidth with an optical signal-to-noise ratio well above 55 dB (0.1 nm ASE noise bandwidth). The corresponding integrated average RIN values for each filtered channel together with the RIN value of the whole spectrum are displayed in figure 4(c). As observed, an integrated average RIN value as low as −152.172 dB Hz^{-1} is obtained in the range from 100 MHz to 10 GHz for the whole optical spectrum. And the noise peak at 3.76 GHz describes the relaxation resonance frequency of the device. Concerning the low power of filtered individual tones, an external PDFA is utilised to pump the signal before RIN measurements. By amplifying each tone to around 5 dBm, the isolated mode demonstrates an integrated average RIN value in the range of −134.955 ∼ −139.179 dB Hz^{-1}, which is sufficiently low and compatible with the requirements for high-speed PAM-4 format transmission systems [55, 56].

The uniformity of the different channels is compared by measuring the 64 Gbaud PAM-4 (128 Gbit s^{-1}) signal transmission in both B2B and 5 km SSMF. Figure 5(a) shows the calculated transmission results versus received optical power for seven carriers under the same bias condition as in figure 4(c) while the figure 5(b) presents the 5 km standard single mode fibre (SSMF) transmission performance for two chosen tones (1290.34 and 1290.86 nm). In both figures, the
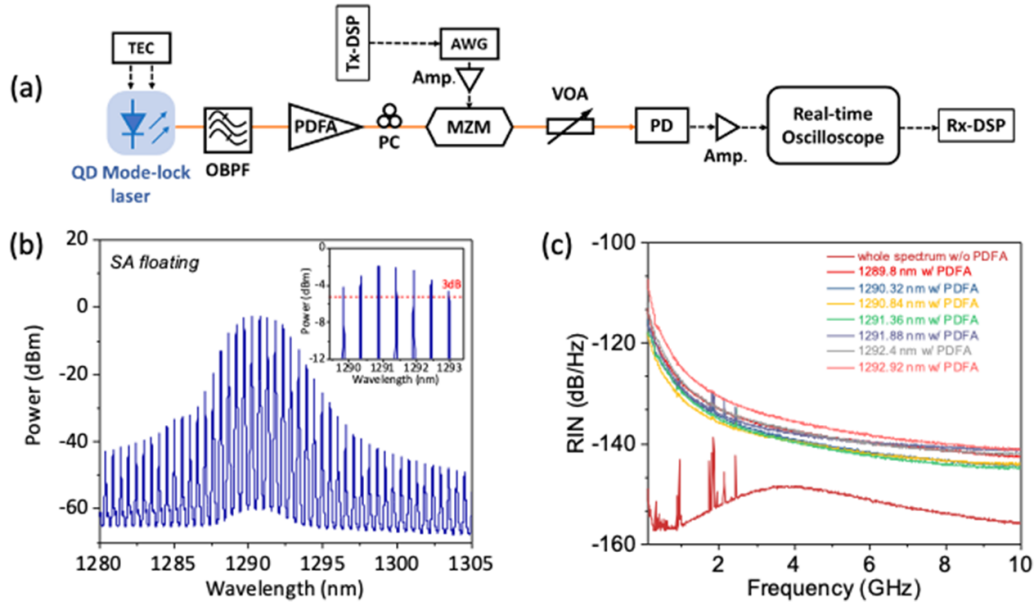
Figure 4. (a) PAM-4 data transmission setup, including DSP, digital signal processing; AWG, arbitrary waveform generator; MZM, Mach–Zehnder modulator; OBPF, optical band pass filter; PC, polarisation controller; VOA, variable optical attenuator; PD, photodetector. (b) Optical combs under bias condition of $I_{gain} = 66$ mA at room-temperature. (c) RIN spectrum of the whole spectrum and the filtered 7 tones within the 3 dB bandwidth in (b).
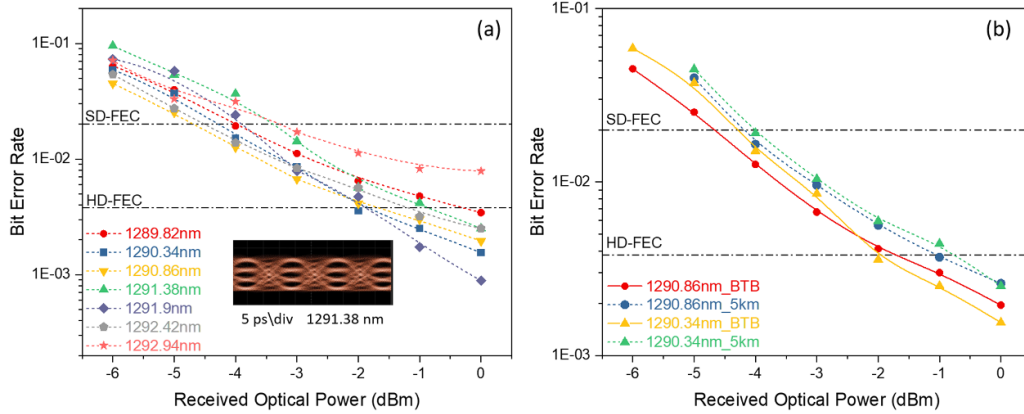
Figure 5. BER performance of 64 Gbaud PAM-4 signal with different comb lines for (a) B2B transmission and (b) 5 km SSMF transmission.

HD-FEC stands for 7% overhead hard decision and the SD-FEC represents the 20% overhead soft decision. As indicated, the BER curves, aside from the one located near the edge at 1292.24 nm, show similar behaviours with the values of BER well-underneath the HD-FEC threshold at 0 dBm received power. The receiver sensitivity of this QD MLL (at BER $= 3.8 \times 10^{-3}$) equals 1.6 dBm and the power penalties for two measured tones are about 1 dB. Meanwhile, the similar slope efficiency and the overlapped points shown in the graph indicate a reasonable consistency of performance between separate channels. The 64 Gbaud PAM-4 electrical eye diagram for channel 1291.38 nm is measured by a digital communication analyser (DCA) (Keysight 86100D DCA-X) and presented in the inset of figure 5(a). The clearly opened eyes suggest a good signal quality in the digital domain.

4. Conclusions

We have developed a wide-spaced OFC source generated by an unbiased passive two-section InAs QD MLL with an ultrahigh fundamental repetition rate. Thanks to the high dot density, good QDs uniformity, as well as the special design of the laser structure, ML is observed with only the current source in a laser cavity as short as 405 μm (corresponding to a mode spacing of 94 GHz between adjacent tones). The nearly-transform-limited pulses can be detected throughout the test range. Meanwhile, the QD-MLL shows excellent intensity noise performance with a typical integrated average RIN value less than -134 dB Hz^{-1} over the frequency range from 100 MHz to 10 GHz. Seven selected wavelengths are utilised as optical carriers to successfully demonstrate a system-level 64 Gbaud PAM-4 (128 Gbit s^{-1}) transmission

experiment. The measured results suggest that our QD-MLL is a compelling candidate as a small footprint, low power consumption, easy operation, and cost-efficient on-chip DWDM light source in the future high-speed PICs.

Data availability statement

The data that support the findings of this study are available upon reasonable request from the authors.

ORCID iDs

Shujie Pan ⬤ https://orcid.org/0000-0001-9122-2060
Mengya Liao ⬤ https://orcid.org/0000-0002-5240-378X
Mingchu Tang ⬤ https://orcid.org/0000-0001-6626-3389
Zihao Wang ⬤ https://orcid.org/0000-0003-4035-1684
Huiyun Liu ⬤ https://orcid.org/0000-0002-7654-8553
Siming Chen ⬤ https://orcid.org/0000-0002-4361-0664

References

[1] Balslev-Clausen D, Ye J, Kirchner M S and Thorpe M J 2008 Cavity-enhanced optical frequency comb spectroscopy: application to human breath analysis *Opt. Express* **16** 2387–97
[2] Bloom B J, Nicholson T L, Williams J R, Campbell S L, Bishof M, Zhang X, Zhang W, Bromley S L and Ye J 2014 An optical lattice clock with accuracy and stability at the 10–18 level *Nature* **506** 71–75
[3] Matsumoto H and Minoshima K 2000 High-accuracy measurement of 240-m distance in an optical tunnel by use of a compact femtosecond laser *Appl. Opt.* **39** 5512–7
[4] Hänsch T W 2006 Nobel lecture: passion for precision *Rev. Mod. Phys.* **78** 1297–309
[5] Hall J L 2006 Nobel lecture: defining and measuring optical frequencies *Rev. Mod. Phys.* **78** 1279
[6] Hodgkinson J and Tatam R P 2012 Optical gas sensing: a review *Meas. Sci. Technol.* **24** 012004
[7] Nugent-Glandorf L, Giorgetta F and Diddams S A 2015 Open-air, broad-bandwidth trace-gas sensing with a mid-infrared optical frequency comb *Appl. Phys.* B **119** 327–38

[8] Liu S, Jung D, Norman J C, Kennedy M, Gossard A C and Bowers J E 2019 A low-noise high-channel-count 20 GHz passively mode locked quantum dot laser grown on Si *Optical Fiber Communication Conf. (OFC) 2019* (*Washington, DC*) (OSA) (https://doi.org/10.1364/OFC.2019.W4E.2)
[9] Delfyett P J, Gee S, Choi M T, Izadpanah H, Lee W, Ozharar S, Quinlan F and Yilmaz T 2006 Optical frequency combs from semiconductor lasers and applications in ultrawideband signal processing and communications *J. Lightwave Technol.* **24** 2701–19
[10] Lundberg L, Mazur M, Mirani A, Foo B, Schröder J, Torres-Company V, Karlsson M and Andrekson P A 2020 Phase-coherent lightwave communications with frequency combs *Nat. Commun.* **11** 201
[11] Marin-Palomo P *et al* 2017 Microresonator-based solitons for massively parallel coherent optical communications *Nature* **546** 274–9
[12] Pfeifle J *et al* 2014 Coherent terabit communications with microresonator Kerr frequency combs *Nat. Photon.* **8** 375–80
[13] Fortier T and Baumann E 2019 20 years of developments in optical frequency comb technology and applications *Commun. Phys.* **2** 153
[14] Diddams S A 2010 The evolving optical frequency comb [Invited] *J. Opt. Soc. Am.* B **27** B51–B62
[15] Wang Z H, Wei W Q, Feng Q, Wang T and Zhang J J 2021 InAs/GaAs quantum dot single-section mode-locked lasers on Si (001) with optical self-injection feedback *Opt. Express* **29** 674–83
[16] Rafailov E U, Cataluna M A and Sibbett W 2007 Mode-locked quantum-dot lasers *Nat. Photon.* **1** 395–401
[17] Stintz A, Liu G T, Li H, Lester L F and Malloy K J 2000 Low-threshold current density 1.3-μm InAs quantum-dot lasers with the dots-in-a-well (DWELL) structure *IEEE Photonics Technol. Lett.* **12** 591–3
[18] Arakawa Y and Sakaki H 1982 Multidimensional quantum well laser and temperature dependence of its threshold current *Appl. Phys. Lett.* **40** 939–41
[19] Pan S *et al* 2020 Quantum dot mode-locked frequency comb with ultra-stable 25.5 GHz spacing between 20 °C and 120 °C *Photon. Res.* **8** 1937
[20] Gosset C, Merghem K, Martinez A, Moreau G, Patriarche G, Aubin G, Ramdane A, Landreau J and Lelarge F 2006 Subpicosecond pulse generation at 134 GHz using a quantum-dash-based Fabry-Perot laser emitting at 1.56 μm *Appl. Phys. Lett.* **88** 241105
[21] Rae A R, Thompson M G, Penty R V, White I H, Kovsh A R, Mikhrin S S, Livshits D A and Krestnikov I L 2006 Harmonic mode-locking of a quantum-dot laser diode *Lasers and Electro-Optics Society Annual Meeting-LEOS Montreal, QC 29/10/06 → 2/11/06* (Institute of Electrical and Electronics Engineers Inc.) (https://doi.org/10.1109/LEOS.2006.279085)
[22] Lu Z G, Liu J R, Raymond S, Poole P J, Barrios P J and Poitras D 2008 312-fs pulse generation from a passive C-band InAs/InP quantum dot mode-locked laser *Opt. Express* **16** 10835–40
[23] Lu Z G, Liu J R, Poole P J, Jiao Z J, Barrios P J, Poitras D, Caballero J and Zhang X P 2011 Ultra-high repetition rate InAs/InP quantum dot mode-locked lasers *Opt. Commun.* **284** 2323–6
[24] Yamamoto N, Akahane K, Kawanishi T, Katouf R and Sotobayashi H 2010 Quantum dot optical frequency comb laser with mode-selection technique for 1-μm waveband photonic transport system *Japan. J. Appl. Phys.* **49** 04DG03
[25] Yamamoto N, Yoshioka Y, Akahane K, Kawanishi T, Sotobayashi H and Takai H 2011 100-GHz channel spacing

and O-band quantum dot optical frequency comb generator with interference injection locking technique *2011 Conf. on Lasers and Electro-Optics: Laser Science to Photonic Applications, CLEO 2011* (IEEE Computer Society) (https://doi.org/10.1364/CLEO_SI.2011.CTuV7)

[26] Kurczveil G, Zhang C, Descos A, Liang D, Fiorentino M and Beausoleil R 2018 On-chip hybrid silicon quantum dot comb laser with 14 error-free channels *Conf. Digest—IEEE Int. Semiconductor Laser Conf.* (*September 2018*) (Institute of Electrical and Electronics Engineers Inc.) pp 79–80

[27] Liu S, Wu X, Norman J, Jung D, Kennedy M, Tsang H K, Gossard A C and Bowers J E 2019 100 GHz colliding pulse mode locked quantum dot lasers directly grown on Si for WDM application *Conf. on Lasers and Electro-Optics* (*Washington, DC*) (OSA) (https://doi.org/10.1364/CLEO_AT.2019.ATu3P.5)

[28] Liu A Y, Srinivasan S, Norman J, Gossard A C and Bowers J E 2015 Quantum dot lasers for silicon photonics [Invited] *Photon. Res.* **3** B1–9

[29] Huang H, Duan J, Jung D, Liu A Y, Zhang Z, Norman J, Bowers J E and Grillot F 2018 Analysis of the optical feedback dynamics in InAs/GaAs quantum dot lasers directly grown on silicon *J. Opt. Soc. Am.* B **35** 2780

[30] Norman J C, Jung D, Wan Y and Bowers J E 2018 Perspective: the future of quantum dot photonic integrated circuits *APL Photonics* **3** 030901

[31] Bimberg D, Grundmann M and Ledentsov N N 1999 *Quantum Dot Heterostructures* (Hoboken, NJ: John Wiley & Sons)

[32] Thompson M G, Rae A R, Xia M, Penty R V and White I H 2009 InGaAs quantum-dot mode-locked laser diodes *IEEE J. Sel. Top. Quantum Electron.* **15** 661–72

[33] Chen S *et al* 2016 Electrically pumped continuous-wave III–V quantum dot lasers on silicon *Nat. Photon.* **10** 307–11

[34] Wei W Q, Feng Q, Guo J J, Guo M C, Wang J H, Wang Z H, Wang T and Zhang J J 2020 InAs/GaAs quantum dot narrow ridge lasers epitaxially grown on SOI substrates for silicon photonic integration *Opt. Express* **28** 26555–63

[35] Yamamoto N, Omigawa K, Akahane K, Kawanishi T and Sotobayashi H 2010 Simultaneous 3 × 10 Gbps optical data transmission in 1-μm, C-, and L-wavebands over a single holey fiber using an ultra-broadband photonic transport system *Opt. Express* **18** 4695–700

[36] Nishi K, Saito H, Sugou S and Lee J-S 1999 A narrow photoluminescence linewidth of 21 meV at 1.35 μm from strain-reduced InAs quantum dots covered by In$_{0.2}$Ga$_{0.8}$As grown on GaAs substrates *Appl. Phys. Lett.* **74** 1111–3

[37] Nishi K, Kageyama T, Yamaguchi M, Maeda Y, Takemasa K, Yamamoto T, Sugawara M and Arakawa Y 2013 Molecular beam epitaxial growths of high-optical-gain InAs quantum dots on GaAs for long-wavelength emission *J. Cryst. Growth* **378** 459–62

[38] Pan S, Cao V, Liao M, Lu Y, Liu Z, Tang M, Chen S, Seeds A and Liu H 2019 Recent progress in epitaxial growth of III–V quantum-dot lasers on silicon substrate *J. Semicond.* **40** 101302

[39] Sooudi E, Huyet G, McInerney J G, Lelarge F, Merghem K, Rosales R, Martinez A, Ramdane A and Hegarty S P 2011 Injection-locking properties of InAs/InP-based mode-locked quantum-dash lasers at 21 GHz *IEEE Photonics Technol. Lett.* **23** 1544–6

[40] Asghar H, Wei W, Kumar P, Sooudi E and McInerney J G 2017 Stabilization of self-mode-locked quantum dash lasers by symmetric dual-loop optical feedback *Opt. Express* **26** 4581–92

[41] Sooudi E, Huyet G, McInerney J G, Lelarge F, Merghem K, Martinez A, Ramdane A and Hegarty S P 2011 Observation of harmonic-mode-locking in a mode-locked InAs/InP-based quantum-dash laser with CW optical injection *IEEE Photonics Technol. Lett.* **23** 549–51

[42] Agrawal G P and Olsson N A 1989 Self-phase modulation and spectral broadening of optical pulses in semiconductor laser amplifiers *IEEE J. Quantum. Electron.* **25** 2297–306

[43] Rafailov E U, Cataluna M A, Sibbett W, Il'inskaya N D, Zadiranov Y M, Zhukov A E, Ustinov V M, Livshits D A, Kovsh A R and Ledentsov N N 2005 High-power picosecond and femtosecond pulse generation from a two-section mode-locked quantum-dot laser *Appl. Phys. Lett.* **87** 081107

[44] Seravalli L, Minelli M, Frigeri P, Allegri P, Avanzini V and Franchi S 2003 The effect of strain on tuning of light emission energy of InAs/InGaAs quantum-dot nanostructures *Appl. Phys. Lett.* **82** 2341

[45] Thomson J D, Summers H D, Smowton P M, Herrmann E, Blood P and Hopkinson M 2001 Temperature dependence of the lasing wavelength of InGaAs quantum dot lasers *J. Appl. Phys.* **90** 4859

[46] Thompson M G, Rae A, Sellin R L, Marinelli C, Penty R V, White I H, Kovsh A R, Mikhrin S S, Livshits D A and Krestnikov I L 2006 Subpicosecond high-power mode locking using flared waveguide monolithic quantum-dot lasers *Appl. Phys. Lett.* **88** 133119

[47] Liu S, Wu X, Jung D, Norman J C, Kennedy M J, Tsang H K, Gossard A C and Bowers J E 2019 High-channel-count 20 GHz passively mode-locked quantum dot laser directly grown on Si with 41 Tbit/s transmission capacity *Optica* **6** 128

[48] Kuntz M *et al* 2004 35 GHz mode-locking of 1.3 μm quantum dot lasers *Appl. Phys. Lett.* **85** 843–5

[49] Tourrenc J P, O'Donoghue S, Todaro M T, Hegarty S P, Flynn M B, Huyet G, McInerney J G, O'Faolain L and Krauss T F 2006 Cross-correlation timing jitter measurement of high power passively mode-locked two-section quantum-dot lasers *IEEE Photonics Technol. Lett.* **18** 2317–9

[50] Nikitichev D I, Ding Y, Ruiz M, Calligaro M, Michel N, Krakowski M, Krestnikov I, Livshits D, Cataluna M A and Rafailov E U 2011 High-power passively mode-locked tapered InAs/GaAs quantum-dot lasers *Appl. Phys.* B **103** 609–13

[51] Thompson M G, Penty R V and White I H 2008 Regimes of mode-locking in tapered quantum dot laser diodes *2008 IEEE 21st Int. Semiconductor Laser Conf.* (IEEE) (https://doi.org/10.1109/ISLC.2008.4635992)

[52] Arkhipov R M, Arkhipov M V and Babushkin I V 2015 On coherent mode-locking in a two-section laser *JETP Lett.* **101** 149–53

[53] Arkhipov R, Pakhomov A, Arkhipov M, Babushkin I and Rosanov N 2021 Stable coherent mode-locking based on π pulse formation in single-section lasers *Sci. Rep.* **11** 1147

[54] Zhang H *et al* 2020 800 Gbit/s transmission over 1 km single-mode fiber using a four-channel silicon photonic transmitter *Photon. Res.* **8** 1776

[55] Lu Z 2019 Quantum-dot coherent comb lasers for terabit optical networking systems *SPIE-Int. Soc. Optical Eng.* (*4 March*) p 22

[56] Eiselt N, Griesser H, Eiselt M, Kaiser W, Aramideh S, Olmos J J V, Monroy I T and Elbers J-P 2017 Real-time 200 Gb/s (4×56.25 Gb/s) PAM-4 transmission over 80 km SSMF using quantum-dot laser and silicon ring-modulator *Optical Fiber Communication Conf.* (*Washington, DC*) vol **part F40-O** (OSA) (https://doi.org/10.1364/OFC.2017.W4D.3)